Energy, Mines and Resources Canada
Énergie, Mines et Ressources Canada

# CANMET

Canada Centre for Mineral and Energy Technology
Centre canadien de la technologie des minéraux et de l'énergie

**Mining Research Laboratories**
**Laboratoires de recherche minière**

[redacted]

Canada

MRL 88-110(TR) C.2

# SOME OBSERVATIONS ON THE ELECTRICAL CHARACTERISTICS OF RADIOACTIVE (RADON PROGENY) AND NON-RADIOACTIVE AEROSOLS

J. BIGU ELLIOT LAKE LABORATORY

MRL 88-110 (TR) MAY 1989

# SOME OBSERVATIONS ON THE ELECTRICAL CHARACTERISTICS OF RADIOACTIVE (RADON PROGENY) AND NON-RADIOACTIVE AEROSOLS

J. Bigu*

Elliot Lake Laboratory, CANMET, Energy, Mines and Resources Canada
P.O. Box 100, Elliot Lake, Ontario, Canada

## ABSTRACT

The electrical characteristics of radon/radon progeny atmospheres have been investigated. Experiments were conducted in a Radon/Thoron Test Facility (RTTF) of the walk-in type using an electrical elutriator of the split-flow variety, originally designed by Johnston. Experiments were carried out with the 'undisturbed' atmosphere, and when this atmosphere was exposed to a source of electrically charged particles produced by a negative ion-generator. Under normal conditions, the average electrical charge of the radon/radon progeny atmosphere was substantially less than one elementary unit. Under the influence of the ion-generator, however, the electrical charge exceeded two elementary units, and the electrical charge distribution was non-symmetrical. It was found that the particle concentration in the RTTF substantially decreased with the operation of the ion-generator.

# INTRODUCTION

The short-lived decay products of radon and thoron are formed initially in an atomic, positively charged state which rapidly combines with sub-micron aerosols. As aerosols are found in positively, negatively and neutrally charged states, the resulting atmosphere consists of a complex mixture of charged and neutral particles of a size covering a wide range.

Similarly, measurements have shown that industrial dusts in the respirable size range also carry an electrical charge (Patterson et al. 1929; Kunkel 1950a and b; Johnston et al. 1985, 1987). The electrical charge associated with Long-Lived Radioactive Dust (LLRD), i.e., dust containing long-lived radioisotopes, is important in the context of this paper. Long-Lived Radioactive Dust is found in mine air in the course of mining operations in uranium mines.

The charge associated with radioactive submicron aerosols and LLRD in the respirable size range is of interest from the health physics standpoint since it influences the deposition of these particles in the human respiratory system (Prodi and Mularoni 1985).

Because of the electrical charge associated with the radon and thoron progenies, and with LLRD, these radioactive particles can be influenced by external electric and magnetic fields (Fuchs 1964; Jonassen 1983; Bigu 1985 and 1986), thereby providing a means to reduce radiation levels in working areas.

The electrical characteristics of radioactive aerosols in their natural environments and non-radioactive aerosols have been investigated by several workers (Billard and Madelaine 1967; Bricard et al. 1964; Dua et al. 1978; Porstendörfer and Mercer 1979; Dua and Kotrappa 1981; Bigu 1985 and 1986; Hoppel 1985). Work on the electrical behaviour and other characteristics of

radon and thoron progeny conducted at our laboratory and in underground uranium mines has been reported elsewhere (Bigu 1983, 1984a, 1985, 1986 and 1988).

This paper deals with the electrical characteristics of a radon/radon progeny atmosphere and with the same atmosphere exposed to a source of electrically charged particles produced by a negative ion-generator. The study has been carried out in a Radon/Thoron Test Facility (RTTF) of the walk-in type. An electrical elutriator of the two split-flow type designed by Johnston el al. (1983) in conjunction with a variety of radioactivity and aerosol measuring instrumentation, has been used in this study.

## DESCRIPTION OF THE APPARATUS

Except for the Radon/Thoron Test Facility (RTTF), and the electrical elutriator, the rest of the instrumentation used in this study is commercially available. An early prototype of the RTTF has been described elsewhere (Bigu 1984b). However, the installation presently used in these experiments is a significantly improved and more flexible version than the one used previously.

The electrical elutriator, heretofore commonly referred to as the Split-Flow Elutriator (SFE), was designed by Johnston (1983) and duplicated at the Elliot Lake Laboratory (Grenier and Butler 1988). A brief description of the elutriator is given below.

The SFE basically consists of two halves that make up the main body of the elutriator, a flow-splitting end cap and two stainless steel parallel plates to which a variable voltage can be applied. The main body and the flow-splitting assembly are made from high-resistivity laminated epoxy resin sheets.

The elutriator channel, lined with the steel plates, is 35 cm in length, 8.6 cm in width, and 0.8 cm in height. Figure 1 shows a side view and

a top cut-away view of the SFE (Johnston 1983).

The size of the SFE channel was designed to operate at a nominal flowrate of 3 $Lmin^{-1}$. This flowrate permits laminar flow conditions in the channel and provides an air clearance time of less than 5 s.

The particular design of the flow-splitting assembly allows the SFE to be used under two different modes of operation of practical interest, namely:

1. Determination of the charge distribution of the aerosol or dust cloud without polarity discrimination: heretofore referred to as configuration X: and
2. Determination of aerosol or dust cloud charge distribution with polarity discrimination, i.e., both polarities are simultaneously measured, heretofore referred to as configuration Y.

In the first case (configuration X), all sampling ports in the flow-splitting assembly are connected together and counted by means of, say, an optical particle counter (for dust) or a condensation nuclei counter (for aerosols).

In the second case (configuration Y), the sampling ports in the flow-splitting assembly of the SFE are connected to two different aerosol or dust concentration monitors, or any similar arrangement for some other specific purpose such as that described in this paper.

## EXPERIMENTAL PROCEDURE

The split-flow elutriator (SFE) was used in configurations X and Y in radon/radon progeny atmospheres produced in the Radon/Thoron Test Facility (RTTF) by means of dry $^{226}Ra$ sources*. In order to minimize plate-out of the radon progeny on the RTTF walls as well as to provide a substrate for

---

*Model RN-1025, Pylon Electronic Development, 147 Colonnade Road, Ottawa, Ontario K2E 7L9.

attachment of the radon progeny, aerosols were injected into the RTTF by means of a constant output aerosol atomizer*, in conjunction with an air supply system**, and other associated equipment. Radon from the $^{226}Ra$ sources was mixed with a NaCl aerosol cloud in a mixing chamber before being injected into the RTTF.

It should be stressed that the SFE cannot distinguish between 'conventional' electrically charged aerosols and electrically charged radon progeny. For this reason it is important to devise a means to ascertain that the electrical charge and electrical charge distribution measured by the SFE correspond to (or are representative of) that of the radon progeny investigated. This can be done using configurations X and Y as illustrated in Figure 2.

In configuration X (top Figure 2), all SFE sampling ports were connected together and then split into two flows: one flow was directed to a condensation nuclei counter $(CNC)^{+}$, whereas the other flow (2.7 $Lmin^{-1}$) went through an absolute filter, housed in a sample holder, by means of a servo-controlled flow adjustable sampling pump. This experimental arrangement permitted monitoring of aerosol concentrations as well as measurement of radon progeny deposited in the filter by gross $\alpha$-counting and $\alpha$-particle spectrometry. Configuration X enabled the study of the electrical characteristics of the 'undisturbed' radon progeny.

In configuration Y, the two sampling sites of the SFE were run independently at 3 $Lmin^{-1}$ each. One side of the SFE flow system was split, as before, into two arms, except that one arm could go either to a CNC or to a Differential Mobility Particle Sizer $(DMPS)^{++}$ in conjunction with a CNC. The DMPS/CNC arrangement was used for aerosol size distribution analysis. The

---

*Model 3076. **Model 3074. $^{+}$Model 3020 (0.3 $Lmin^{-1}$). $^{++}$Model 3071, Thermo-Systems Inc., (T.S.I.), P.O. Box 43394, St. Paul, MN 55164.

other arm was connected to a sample holder/filter arrangement for radioactivity measurement purposes. The second sampling site of the SFE could be connected to a similar arrangement to that described for the first site, or alternatively to a CNC for aerosol monitoring purposes, or to operate in the conventional way described in the literature (Johnston 1983; Johnston et al. 1985, 1987). It should be noted that configuration Y can also be realized by using one sampling site of the SFE in the manner described above while maintaining the other side at the same airflow by means of an external pump. Charge distribution information can be obtained by alternatively reversing the polarity of the voltage applied to the plates of the SFE or by running a series of measurements with one polarity first, and then reversing the polarity.

Configuration Y was used to investigate the electrical characteristics of radon progeny exposed to a source of negatively charged ions produced by a small ion-generator*. The negative ion-generator provided a means to deposit electrical charge on radon progeny. Configuration Y is shown in Figure 2 (bottom).

Measurements with the SFE were made by varying the external DC voltage applied to the SFE plates between 0 and $\pm$5000 V. The DC voltage was provided by an external DC power supply.

In addition to the above, frequent measurements of aerosol concentration and size distribution in the RTTF were made.

## THEORETICAL BACKGROUND

It can be shown that the number of elementary charges, n, on a particle is given by (Johnston 1983, Hochrainer 1985).

---

*Model Bionair 100A, Bionair Corporation, 565A Commerce St., Flankling Lakes, NJ 07417.

$$n = 3\pi\mu\eta D_p/eC \qquad \text{Eq 1}$$

where, $\eta$ is the air viscosity (~$1.8 \times 10^{-5}$ Kg $s^{-1}$ $m^{-1}$)

$D_p$ is the particle diameter (m)

$\mu$ is the particle mobility ($m^2$ $V^{-1}$ $s^{-1}$)

e is the electron charge ($1.602 \times 10^{-19}$ Coulomb)

C is the Cunningham slip correction (~1)

The mobility of the particle can be obtained from the flowrate conditions and the physical dimensions of the SFE as follows (Johnston 1983):

$$\mu = F(Q/V_o) \qquad \text{Eq 2}$$

where, Q is the sampling flowrate ($m^3$ $s^{-1}$)

F is a geometrical factor given by b/wl

where, b, w and l are the physical dimensions of the SFE (i.e., w and l, are, respectively, the channel width and the channel length, whereas b is half the SFE channel height. All dimensions in m).

$V_o$ is a voltage defined as follows: particle concentration data are tabulated as a function of voltage differential applied to the SFE. The data are then normalized to zero volt concentration and plotted. A tangent passing through the 50% normalized concentration point defines the voltage $V_o$ by drawing a vertical line to the x-axis (i.e., voltage) from the tangent contact point (see Figure 3).

Substituting Equation 2 into Equation 1, one gets the number of elementary charges on a particle size $D_p$:

$$n = 3\pi FK(D_p/V_o) \qquad \text{Eq 3}$$

where,

$$K = \eta Q/eC \qquad \text{Eq 4}$$

Taking into account that for the SFE used here, w = $8.6 \times 10^{-2}$ m, l = 0.35 m, and b = $4 \times 10^{-3}$ m, it can be shown that Equation 3 reduces to:

$$n = 7.036 \times 10^9 \ (D_p/V_o) \qquad \text{Eq 5}$$

where, $D_p$ is in meter.

The procedure outlined above (Johnston 1983) can be applied to particles of different sizes in an aerosol or dust cloud in order to obtain the electrical charge distribution of the cloud. This procedure is straight forward for clouds with symmetrical charge distributions. However, for non-symmetrical charge distributions, the procedure is more complex as described elsewhere (Johnston 1983).

## EXPERIMENTAL RESULTS AND DISCUSSION

It is important in the context of the data presented here to distinguish between the meaning given in this paper to 'total' aerosol and radioactive aerosol. In the first category both radioactive (in this case radon and its progeny) and non-radioactive aerosols are included, whereas in the second category only radon progeny aerosols (free or attached to other non-radioactive aerosols) are considered. Although it should be evident that radioactive and non-radioactive aerosols are all part of the same particle distribution, the above terminology is useful and justifiable because the radioactive aerosol distribution can, in fact, be determined experimentally (see below), and hence, distinguished from non-radioactive aerosols.

Because the SFE cannot distinguish between the two categories on the basis of charge, an experimental protocol was designed, as previously indicated, to identify, characterize, and quantify both components, namely the radioactive and non-radioactive aerosol fractions in the 'total' aerosol cloud. For simplicity, the experimental data will be divided into the following groups:

a) Electrical characteristics of the total aerosol cloud, without external electrical influence, i.e., no ion-generator;

b) Electrical characteristics of the radioactive aerosol cloud, without external electrical influence, i.e., no ion-generator:

c) Electrical characteristics of the total aerosol cloud under the influence of an ion-generator; and

d) Electrical characteristics of the radioactive aerosol cloud under the influence of an ion-generator.

## A. ELECTRICAL CHARACTERISTICS OF TOTAL AEROSOL (NO ION-GENERATOR)

Figures 3 to 5, and Tables 1 and 2 show data obtained using the SFE in configuration X in conjunction with the CNC (Figure 2), and the DMPS/CNC arrangement (Figures 4 and 5).

Figure 3 shows the total aerosol concentration versus high voltage (H.V.). Only the negative portion of the graph is shown because the aerosol cloud was symmetrical with respect to charge. (The same was found to hold true for the radioactive aerosol, where Table 2 shows the radon progeny concentration versus several positive and negative values of the H.V. on the SFE to illustrate this point.)

Figure 4 shows the total aerosol concentration size distribution for two SFE voltage conditions, namely 0 V and -2000 V. This Figure and Table 1 show that the geometric mean (G.M.) of the size distribution after passing through the SFE decreases with increasing voltage. For the particular experimental conditions, an example is given in Figure 4, a decrease in G.M. of ~19% was brought about by the application of -2000 V. The percentage reduction in the G.M. of the aerosol cloud depends on the voltage applied to the SFE, experimental conditions, type of aerosol, water vapour content, and possibly other characteristics of the aerosol cloud, in a little understood fashion.

A decrease in the G.M. of the aerosol cloud suggests the removal of the larger particle size fraction from the aerosol size distribution. However, as the electrical force exerted on a charged particle is proportional to the

electrical charge on the particle, a reduction in G.M. of the charged aerosol cloud can be interpreted as the removal of the fraction of particles with higher electrical charge. Hence, from particle size and electrical charge (on the particle) considerations one may surmise that Figure 4 and Table 1 demonstrate that under our experimental conditions large particles carry, in general, more charge than smaller particles.

A value for the electrical charge of the aerosol cloud can be estimated from the Figure by following Johnston's graphical procedure described elsewhere (Johnston 1983: Johnston et al. 1985). This procedure consists of drawing a straight line from the y-axis corresponding to $N_0/2$ (where $N_0$ is the total aerosol concentration corresponding to 0 V) tangent to the aerosol concentration (N) versus H.V. curve. The intersection point is then projected onto the x-axis where the corresponding voltage, $V_0$, is read. The voltage so obtained is then substituted into Equation 5 in order to obtain n, the electrical charge. Figure 3 gives $V_0 \sim 4 \times 10^3$ V.

Because Figure 3 has been obtained with a CNC (which measures aerosol concentration but provides no particle size distribution information, except for approximate lower and upper particle size operating limits), the value for n is not defined unless a definite particle size is chosen to describe the aerosol cloud. An obvious choice is the G.M. of the aerosol cloud. Taking G.M. = 0.09 $\mu$m, as an approximate value based on experimentation, and H.V. = $5 \times 10^3$ V, and substituting this value into Equation 5, one gets:

$$n = 7.036 \times 10^9 \ (0.09 \times 10^{-6}/4 \times 10^3) \sim 0.16$$

Since the electrical charge on a particle is either 0 or an integer, values for n less than unity suggest that a fraction of the aerosol cloud carries no electrical charge. Figure 3 indicates that over 50% of the aerosol cloud is electrically charged. (Most likely >60% if the line is extrapolated to H.V. > $5 \times 10^3$ V). This value is consistent with other experimental work

by the author (Bigu 1985; Bigu and Grenier 1986).

As indicated above the value n ~0.16 obtained above is not truly representative of the electrical charge of the aerosol cloud because particle size distribution information is not given. A more accurate electrical charge description of the aerosol cloud can be obtained by substituting the CNC by the DMPS/CNC arrangement, and conducting a similar kind of analysis covering the entire particle size range in small particle size increments. The result of such analyses is summarized in Figure 5 where n (see Equation 5) is plotted versus $D_p$ (particle size, $\mu$m). This graph shows that the electrical charge on the particle varies with particle size ranging from ~0.15 for $D_p$ ~0.07 $\mu$m to ~1.2 for $D_p$ ~0.34 $\mu$m. Data for $D_p > 0.35$ $\mu$m are not reliable because of the low particle concentration in this size range, and hence, poor statistics of counting. The decrease of n for $D_p > 0.3$ $\mu$m is not clearly understood, but may be caused by a combination of poor counting statistics, bias of the DMPS, and other as yet unknown factors. Figure 5 shows that except for $D_p > 0.35$ $\mu$m, the particle electrical charge increases with the particle size.

## B. ELECTRICAL CHARACTERISTICS OF RADIOACTIVE AEROSOLS (NO ION-GENERATOR)

Figures 6 and 7, and Tables 1 and 2 show radioactive aerosol data using the SFE in configuration X in conjunction with the DMPS/CNC arrangement. In this case, the outlet of the SFE was split into two arms by means of a 'Tee', one of which (0.3 $Lmin^{-1}$) was connected to the DMPS/CNC system whereas the other was connected to a filter holder, housing a filter, and a pump which sampled aerosol at a rate of 2.7 $Lmin^{-1}$ (see Figure 2, top). The total flowrate through the SFE was 3 $Lmin^{-1}$, as before.

The sampling filter was used to collect radioactive aerosol, i.e., radon progeny, and the DMPS/CNC to gather, concurrently, total aerosol and particle size distribution data (Table 1). Radioactive aerosol was sampled

for 5 min at a time at different H.V. and the α-particle activity was measured by α-spectrometry using a silicon-barrier detector, and associated electronic circuitry, in conjunction with a multichannel analyzer. The spectra so obtained (i.e., $^{218}Po$ and $^{214}Po$ photopeaks) were used in the analysis. Radon progeny and total aerosol data are shown in Table 1 and plotted in Figure 6. (It should be noted that the integrated α-particle count under the $^{218}Po$ and $^{214}Po$ photopeaks as well as the total α-count, i.e., $^{218}Po$ + $^{214}Po$, have been plotted independently in Figure 6. The normalized α-counts are, however, very similar and for all practical purposes they can be considered identical. Because of this, a single line passing through all radon progeny data points has been drawn.)

An estimate for the electrical charge of the radon progeny aerosol cloud can be obtained by applying Johnston's method to the α-particle count following the same procedure as for the total aerosol concentration (see case A and Figure 3). The value obtained for $V_o$ is ~1640 V (see Figure 6). Unfortunately, the experimental arrangement used did not allow for the radon progeny size distribution to be determined. This can be done using diffusion batteries of the screen, parallel plate, or concentric type. However, concurrent radon progeny size distribution measurements would have made the present experiment far too complex as not all the necessary variables of interest could have been determined simultaneously.

It is well known that for a lognormal aerosol distribution radon progeny attach themselves preferentially to airborne particles in the submicron size range (<0.1 to ≲0.2 μm) (Mercer and Stowe 1971). This value and the G.M. for the total aerosol cloud are similar enough so that $D_P$ ~0.1 μm can be taken in the calculations for comparison purposes. Using Equation 5, one obtains n ~0.43 for radon progeny. For the total aerosol cloud $V_o$~ 4 x $10^3$ V (see Figures 3 and 6), hence n ~0.16 is obtained. Assuming similar size

distributions for the total aerosol and radon progeny clouds, the above results suggest that radon progeny carry an electrical charge ~2.5 times larger than 'normal' (i.e., non-radioactive) aerosol. This result can be understood because of aerosol self-charging effects caused by radioactive decay (Yeh 1976). Furthermore, because the electrical charge carried by radon progeny must be either 0 or an integer, $n < 1$ indicates that a fraction of the radon progeny cloud carries no electrical charge. From Figure 6 it can be seen that about 65% of the radon progeny is either positively or negatively charged whereas the remaining fraction (~35%) is in a neutrally charged state. These data are consistent with other measurements by the author (Bigu 1985, 1986).

Figure 7 shows radon progeny spectra at three different voltages, namely, 0 V, -500 V, and -2000 V. The spectra show a decrease of the $^{218}Po$ and $^{214}Po$ photopeaks with increasing H.V., as previously discussed (Table 1 and Figure 6). No significant spectral difference as measured by the ratio $^{218}Po/^{214}Po$ were found.

Table 2 shows that N and radon progeny data are equally affected by a given H.V. either positive or negative. Other relevant data are also shown in this Table.

From Figures 6 and 7, and Tables 1 and 2, one may tentatively surmise:

1. The electrical charge on radon progeny appears to be significantly larger than that corresponding to the total aerosol cloud;
2. Both $^{218}Po$ and $^{214}Po$ are electrically charged;
3. About 65% of the radon progeny are electrically charged either positively or negatively.

## C. ELECTRICAL CHARACTERISTICS OF TOTAL AEROSOL UNDER THE INFLUENCE OF AN ION-GENERATOR

In this study, the total aerosol cloud was exposed to a negative ion-generator (IG) in order to induce charge effects, i.e., to deposit electrical charge on the particles forming the cloud. Particle size and charge distributions of the aerosol cloud under the influence of the ion-generator were determined. The effect of the ion-generator could not be anticipated because of the lack of technical information by the manufacturer of the IG. The manufacturer claims that the IG produces a large excess of negative ions. However, the kind of ions, particle size and electrical charge distributions are not available.

In this study it was important to determine the electrical polarity of the particles. Hence, configuration Y (Figure 2, bottom) was used. The results of this investigation are shown in Figures 8 to 10, and Tables 3 and 4.

Figure 8 shows the aerosol concentration, N, measured with the CNC versus positive and negative voltage applied to the SFE. Contrary to data obtained without the IG, the experimental results obtained using the IG are markedly charge asymmetric.

Although the DMPS/CNC apparatus was used occasionally in this series of experiments, the data shown in Figure 8 were obtained with the CNC. The relatively long time required by the DMPS/CNC apparatus to acquire, process, and print-out particle mobility and size distribution data was not particularly suitable for the experiment with the IG where a large number of measurements had to be carried out in a short time with the IG on and off, and within a wide range of positive and negative values for the voltage. Hence, the analysis that follows from Figure 8 is done by taking the G.M. of the aerosol cloud (i.e., ~0.085 $\mu$m as determined by the DMPS/CNC arrangement).

This value for the G.M. represents an average because it varies with experimental conditions, e.g., operation of the IG. (A more accurate procedure would have entailed a series of similar measurements for each particle size using the DMPS/CNC apparatus. The reasons for not having done so have been given above.)

Because of the asymmetrical nature of the graph describing N versus H.V. (positive and negative), the simple graphical procedure used before to obtain $V_o$ and, hence, n, can no longer be applied. In the present case 'deconvolution' of the data of Figure 8 was done using a graphico-analytical method developed by Johnston (1983) designed to deal with charge asymmetric situations (see Appendix). The result of this analysis is presented in Figure 9. This graph shows that a large fraction of the aerosol cloud is charged negatively under the influence of the ion-generator with an electrical charge of about 2.34 $\pm$ 0.5 elementary units corresponding to particles with electrical mobility of ~2.5 x $10^{-8}$ $m^2$ $V^{-1}$ $s^{-1}$. (If, for rough comparison purposes, the simplified graphical analysis used in Sections A and B is applied to the positive and negative voltage portions of Figure 8 independently, the following, respective, values for $V_o$ are obtained (using Equation 5 for $D_p$ = 0.085 $\mu$m): $V_o(+)$ = 1.5 and $V_o(-)$ = 3.0. The mean value of $V_o(+)$ and $V_o(-)$ is 2.25 which does not differ much from n = 2.34 $\pm$ 0.5 given above. Alternatively, n = 2.34 $\pm$ 0.5 obtained by the rigorous method is somewhere between $V_o(+)$ and $V_o(-)$.)

Figure 10 shows the total aerosol size distribution in the RTTF (bypassing the SFE) when the IG is off (top left hand side histogram) and when the IG is operating (bottom left hand side histogram). The right hand side histograms of Figure 10 show the total aerosol size distribution using the SFE when a voltage of -5000 V is applied with the IG off (top histogram), and when the IG is on (bottom histogram).

The data of Figure 10 show that the aerosol concentration in the RTTF is reduced by the operation of the IG, an experimental fact that has been observed by the author in the course of several studies (Bigu 1983, 1984a and 1988). The reduction in aerosol concentration was in the range 10-20% (see also Table 3) with no apparent significant difference in the G.M. of the distribution. The latter is to be expected because of the limited ion output of the IG and the relatively large volume of the RTTF (~30 $m^3$). The modest reduction in N in the RTTF is consistent with the above, and hence the constancy of G.M.. The reduction in aerosol concentration in the RTTF when the IG was on could tentatively be attributed to an increase in charged aerosol plate-out on the RTTF walls. (Plate-out of charged aerosols on plastic tubing walls, and other apparatus surfaces could also contribute significantly but this effect has not been investigated here, and hence is an unknown variable.)

A considerable reduction (10-20 fold) in aerosol concentration was observed at the outlet of the SFE in the voltage range 0 to -5000 V when the IG was operated in close proximity to the SFE (see Table 4). Furthermore, the G.M. of the aerosol distribution was significantly reduced (~30% for H.V. ~ -5000 V, ~20-25% for H.V. = 0 V) by the operation of the IG (see bottom of Table 4). This effect persisted even at 0 voltage where an average G.M. ~0.0877 $\mu$m was obtained when the IG was off compared with a value of 0.0661 $\mu$m when the IG was on.

The observed reduction in N and G.M. of the irradiated aerosol cloud when using the SFE can, tentatively, be interpreted as the product of clustering, condensation or coagulation of small charged and neutral particles into larger (charged) ones, which are, therefore, more easily removed by the SFE on account of their larger electrical charge on their surface. The net effect of the IG in the RTTF is a reduction in N (which has been

experimentally verified as indicated above), and an increase in G.M. which can indirectly be inferred from SFE data.

The effect of the IG on N versus voltage (H.V.) is also shown in Figure 12 (which also shows the total radon progeny $\alpha$-particle count as discussed in Section D. below). An estimate of the electrical charge on the aerosol cloud calculated for the negative voltage portion of the Figure and Equation 5. assuming G.M. ~0.085 $\mu$m, gives n ~ 2.7 elementary unit charges, which is in fair agreement with other values given above.

## D. ELECTRICAL CHARACTERISTICS OF RADIOACTIVE AEROSOLS UNDER THE INFLUENCE OF AN ION-GENERATOR

Data regarding the electrical characteristics of radon progeny in the RTTF have been summarized in Figures 11 to 13 and Table 4. As for total aerosol. the characteristics of the radon progeny under the influence of the IG were investigated using the SFE in configuration Y. However, because of severe practical constraints. experimental difficulties and time limitations. the polarity of the radioactive aerosol could not be investigated in detail as in Section C for the total aerosol. Hence. data obtained when negative voltages were applied to the SFE are presented here. The analysis carried out with these data is similar to that of sections A and B.

Figure 11 shows the normalized $\alpha$-particle count versus H.V. for $^{218}Po$. $^{214}Po$. and $^{218}Po$ + $^{214}Po$. i.e., total $\alpha$-count under the two photopeaks. denoted by $N_{\alpha,T}$. As for the case discused in Section B, radon progeny were analyzed by $\alpha$-spectrometry. Figure 12 shows $N_{\alpha,T}$ versus H.V. Also shown in this graph. for comparison purposes. is the total aerosol concentration versus H.V..

Calculation of the electrical charge for the radon progeny assuming $D_p$ ~G.M. = 0.085 - 0.1 $\mu$m (see Table 4 and other calculations in this paper).

and applying the values for $V_o$ obtained from Figure 11 to Equation 5, gives n ~2.4 to 3.5 for the electrical charge on radon progeny under the influence of the ion-generator. The above range of values for n is significantly higher than that obtained with the IG off (see Section B).

Figure 12 shows the normalized total aerosol concentration (N) and total $\alpha$-particle activity ($N_{\alpha,T}$) versus voltage (H.V.) for an experiment in the RTTF with the IG on. For this particular experiment $n(N_{\alpha,T}) < n(N)$ ~4.0.

Because of the inherent error associated with the graphical method and other considerations regarding particle size distribution discussed earlier, the results given above are only approximate and may be expected to vary depending on aerosol composition, method of aerosol production, local environmental conditions in the RTTF, water content of the aerosol cloud, and other factors.

Figure 13 shows radon progeny $\alpha$-particle spectra obtained using the SFE with no voltage for the IG off (top graph) and when the IG has been operating for a short period (bottom graph). A dramatic decrease in radon progeny collected on the sampling filter can be observed, caused by the operation of the IG (see also Table 4). This decrease in $\alpha$-particle activity is presumably similar to the decrease in N for the total aerosol cloud, as discussed above.

## CONCLUSIONS

Some of the main conclusions that can be derived from this study are the following:

1. For the undisturbed aerosol cloud (i.e., IG off), the electrical charge distribution was symmetrical and $0 < n < 1$ with n(total aerosol cloud) <n(radon progeny). Furthermore, ~50% of the total aerosol cloud and ~65% of the radioactive aerosol (radon progeny) were electrically charged as evidenced by SFE data;

2. For the disturbed aerosol cloud (i.e., IG on), the electrical charge was non-symmetrical. Over 90% of the cloud was electrically charged with an average charge, n >2. Furthermore, the total aerosol and radon progeny concentrations decreased and the G.M. of the total aerosol cloud increased, as indicated by SFE data.

It should be noted that an increase in particle (radioactive and non-radioactive aerosol) plate-out on the RTTF walls and the SFE plates, caused by the operation of the ion-generator, has not been considered here, but should not be ignored. Because of practical constraints, no concurrent plate-out measurements were conducted in order to ascertain the importance of this phenomenon on the effects observed. A continuation of the present studies with different kinds of instrumentation are in progress in order to further verify and improve the data presented here. Plate-out measurements are planned to determine its role on the phenomena subject of this paper.

## ACKNOWLEDGEMENTS

The author would like to thank E. Edwardson for his experimental assistance in this project. Thanks are also extended to M. Grenier, who duplicated the Johnston's SFE apparatus in our laboratory, for helpful discussions regarding the performance of the spectrometer.

## REFERENCES

Bigu, J. On the effect of a negative ion generator and a mixing fan on the plate-out of radon decay products in a radon box. Health Phys. 44:259-266; 1983.

Bigu, J.: Grenier, M. On the effect of a negative ion generator and a mixing fan on the attachment of thoron-decay products in a thoron box. Health Phys. 46|:933-939: 1984a.

Bigu, J. A walk-in radon/thoron test facility. Am. Ind. Hyg. Assoc. J. 45:525-532; 1984b.

Bigu, J. Effects of electric fields on $^{220}Rn$ progeny concentration. Health Phys. 49:512-516; 1985.

Bigu, J.; Grenier, M. Electrical characteristics of the short-lived decay products of thoron in underground uranium mines. Am. Ind. Hyg. Assoc. J. 47:308-311; 1986.

Bigu, J. Effect of selected variables on airborne $^{220}Rn$ progeny concentrations. Health Phys. 54:93-98; 1988.

Billard, F; Madelaine, G. Etude de la charge electrique portee par les aerosols. In: Assessment of airborne radioactivity, proceedings of a symposium held by the International Atomic Energy Agency. Vienna: IAEA: EAEA-SM-95/13; 1967: 325-333.

Bricard, J.; Renoux, A; Pradel, J; Madelaine, G. Spectre des aerosols naturels radioactifs. In: La pollution radioactive des milieux gazeux. pp 15-17; 1964.

Dua, S.K.; Kotrappa,P.: Bhanti, D.P. Electrostatic charge on decay products of thoron. Am. Ind. Hyg. Assoc. J. 39:339-345; 1978.

Dua. S.K.: Kotrappa, P.; Comment on the charge on decay products of thoron and radon. Am. Ind. Hyg. Assoc. J. 42:242-243; 1981.

Fuchs, N.A. The mechanics of aerosols. New York: The Macmillan Company; 1964.

Grenier, M.G.; Butler, K. Evaluation of a split-flow elutriator used in the determination of airborne dust charge distributions. Elliot Lake Laboratory (CANMET, Energy, Mines and Resources Canada); 1988. Ottawa, Canada. Mining Research Laboratories Division Report MRL 87-187(TR).

Hochrainer, D. Measurement methods for electric charges on aerosols. Ann. Occup. Hyg. 29:241-249; 1985.

Hoppel, W. Ion-aerosol attachment coefficients, ion depletion, and the charge distribution on aerosols. J. of Geophys. Res. 90:5917-5923; 1985.

Johnston, A.M. A semi-automatic method for the assessment of electric charge carried by airborne dust. J. Aerosol Sci. 14:643-655; 1983.

Johnston, A.M.; Vincent, J.H.; Jones, A.D. Measurements of electric charge for workplace aerosols. Ann. Occup. Hyg. 29:271-284; 1985.

Johnston, A.M.; Vincent, J.H.; Jones, A.D. Electrical charge characteristics of dry aerosols produced by a number of laboratory mechanical dispensers. Aerosol Sci. & Tech. 6:115-127; 1987.

Jonassen, N. The effect of electric fields on $^{222}Rn$ daughter products in indoor air. Health Phys. 45:487-491; 1983.

Kunkel, W.B. The static electrification of dust particles on dispersion into a cloud. J. Appl. Phys. 21:820-832; 1950a.

Kunkel, W.B. Charge distribution in coarse aerosols as a function of time. J. Appl. Phys. 21:833-837; 1950b.

Mercer, T.T.; Stowe, Wm. Radioactive aerosols produced by radon in room air. In: Inhaled particles III. volume 2 (W.H. Walton, Ed.) Surrey (England) Unwin Bros. Ltd. 839-851; 1971.

Patterson, H.S.; Whytlaw-Gray, R.; Cawood, W. The structure and electrification of smoke particles. Proc. Roy. Soc. A 124:523-532, 1929.

Porstendörfer, J.; Mercer, T.T. Influence of electric charge and humidity upon the diffusion coefficient of thoron decay products. Health Phys. 37: 191-199; 1979.

Prodi, V; Mularoni, A. Electrostatic lung deposition experiments with humans and animals. Ann. Occup. Hyg. 29:229-240; 1985.

Yeh, H. A theoretical study of electrical discharging of self-charging aerosols. J. Aerosol Sci. 7:343-349; 1976.

Table 3 - Effect of a negative ion-generator on aerosol concentration in a Radon/Thoron Test Facility of the walk-in type. No SFE used.

| Time | N ($cm^{-3}$) | $N_{nor}$ | IG | $D_P(N_{max})$ ($\mu m$) | G.M. ($\mu m$) |
|---|---|---|---|---|---|
| 12:48 | 8103 | 0.787 | ON | 0.107 | 0.0917 |
| 13:56 | 8135 | 0.790 | ON | 0.093 | 0.0906 |
| 14:45 | 9622 | 0.934 | OFF | 0.107-0.124 | 0.0897 |
| 15:33 | 9175 | 0.891 | ON | 0.093-0.107 | 0.0911 |
| 16:36 | 10300 | 1.000 | OFF | 0.093-0.107 | 0.0890 |

Notes: N stands for aerosol concentration. $N_{nor}$ represents the normalized aerosol concentration relative to the maximum N measured. The symbol IG stands for ion-generator. $D_P(N_{max})$ represents the diameter corresponding to the maximum aerosol concentration in the aerosol cloud. G.M. stands for geometric mean.

LIST OF ILLUSTRATIONS

Figure 10. Total aerosol size and concentration distributions in the RTTF with IG off and on (left hand side histograms, top and bottom, respectively). Also shown are data at the outlet of the SFE for H.V. = -5000 V with IG off and on (right hand side histograms).

Figure 11. Normalized $\alpha$-particle count versus SFE voltage for $^{218}Po$, $^{214}Po$, and total $\alpha$-particle count ($N_{\alpha,T}$).

Figure 12. Normalized total aerosol concentration (N) and $\alpha$-particle count ($N_{\alpha,T}$) versus SFE voltage.

Figure 13. Alpha-particle spectra at the outlet of the SFE for H.V. = 0 V, and IG off (top) and IG on (bottom). Aerosol cloud exposed to a negative ion-generator.

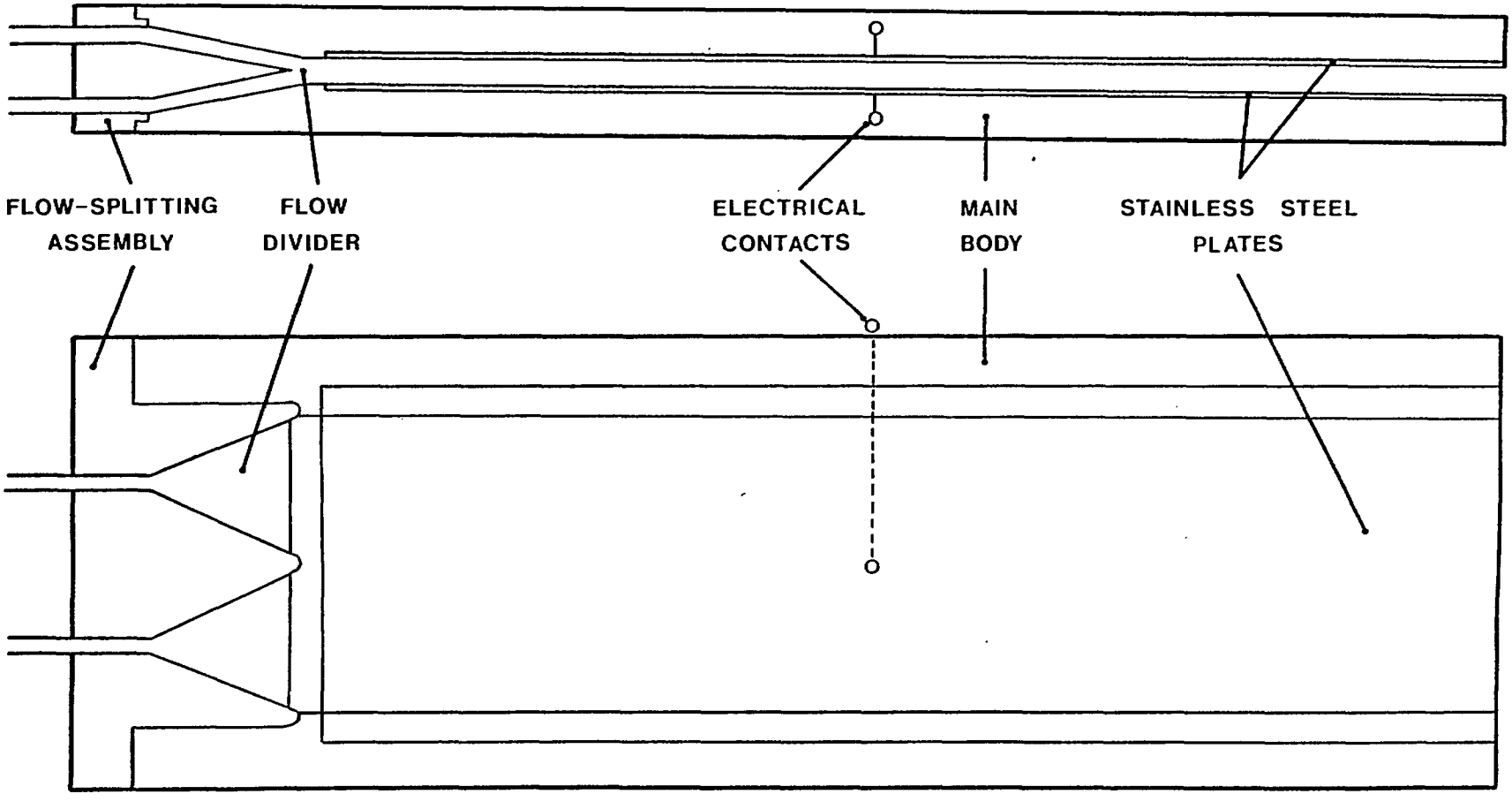
FLOW-SPLITTING ASSEMBLY
FLOW DIVIDER
ELECTRICAL CONTACTS
MAIN BODY
STAINLESS STEEL PLATES

Figure 1.

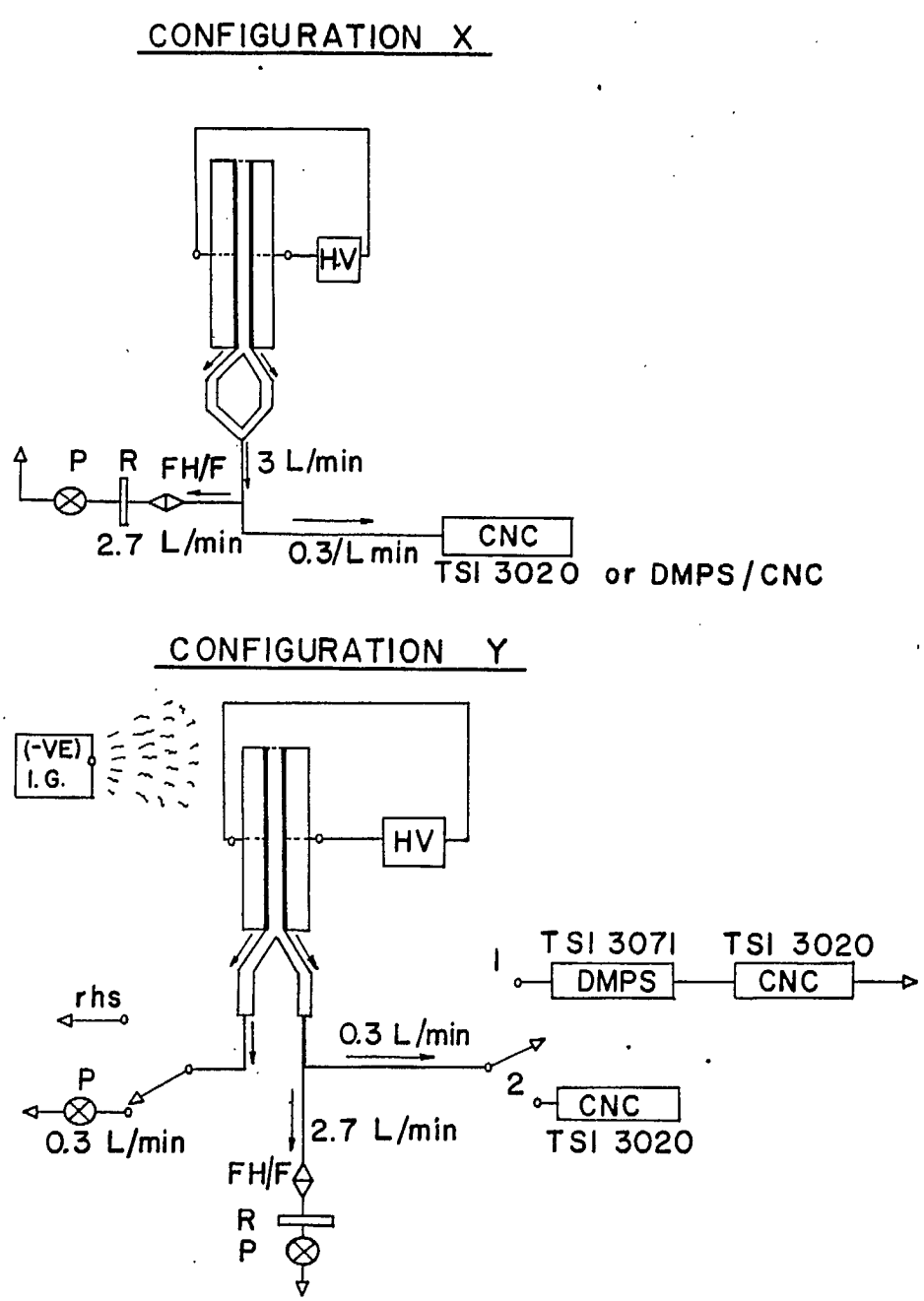
CONFIGURATION X
HV
P
R
FH/F
3 L/min
2.7 L/min
0.3/L min
CNC
TSI 3020 or DMPS/CNC
CONFIGURATION Y
(-VE)
I.G.
HV
TSI 3071
TSI 3020
1
DMPS
CNC
rhs
0.3 L/min
P
2
CNC
TSI 3020
0.3 L/min
2.7 L/min
FH/F
R
P

Figure 2.

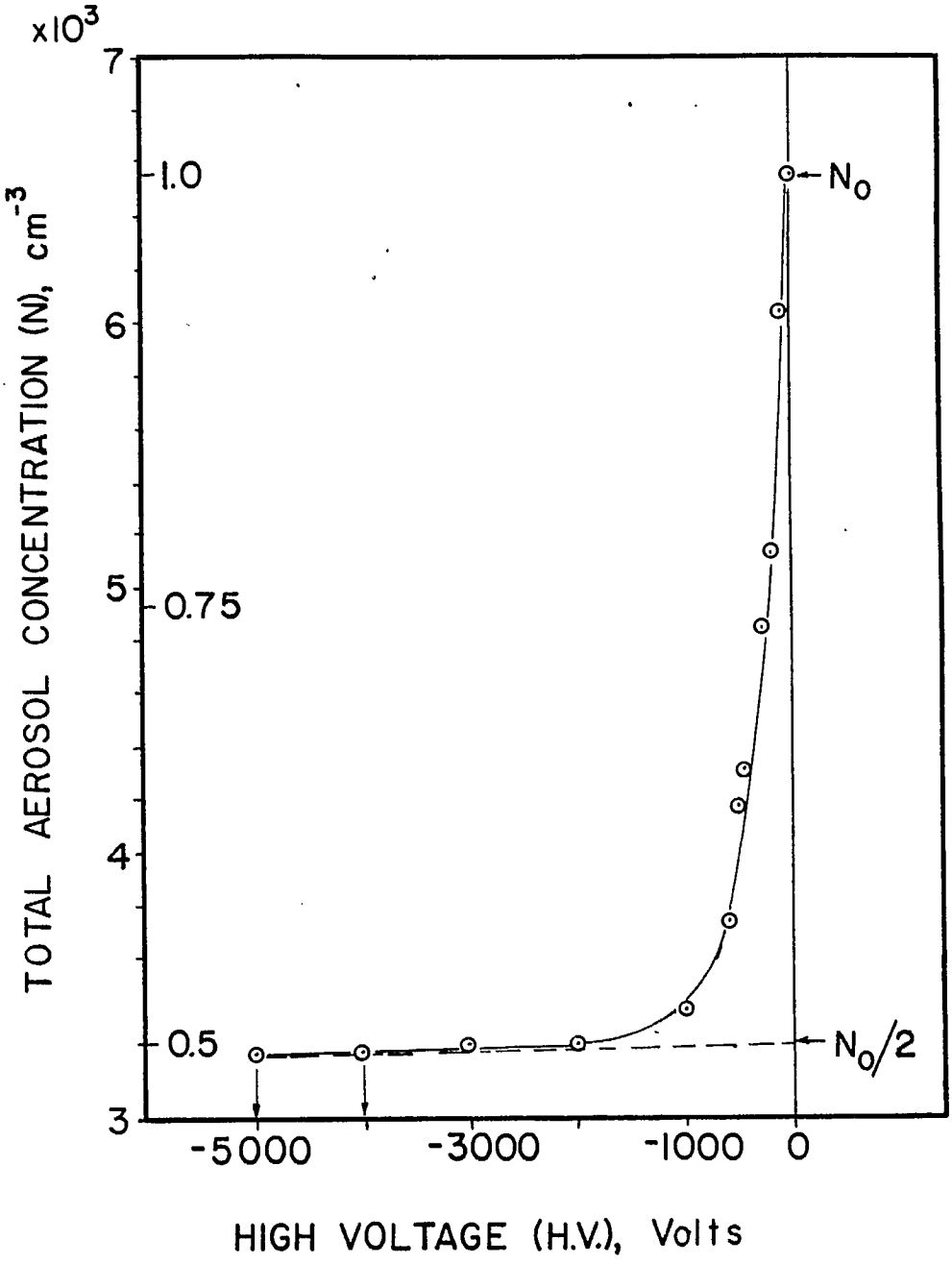
x10³
7
6
5
4
3
1.0
0.75
0.5
N₀
N₀/2
TOTAL AEROSOL CONCENTRATION (N), cm⁻³
-5000
-3000
-1000
0
HIGH VOLTAGE (H.V.), Volts

Figure 3.

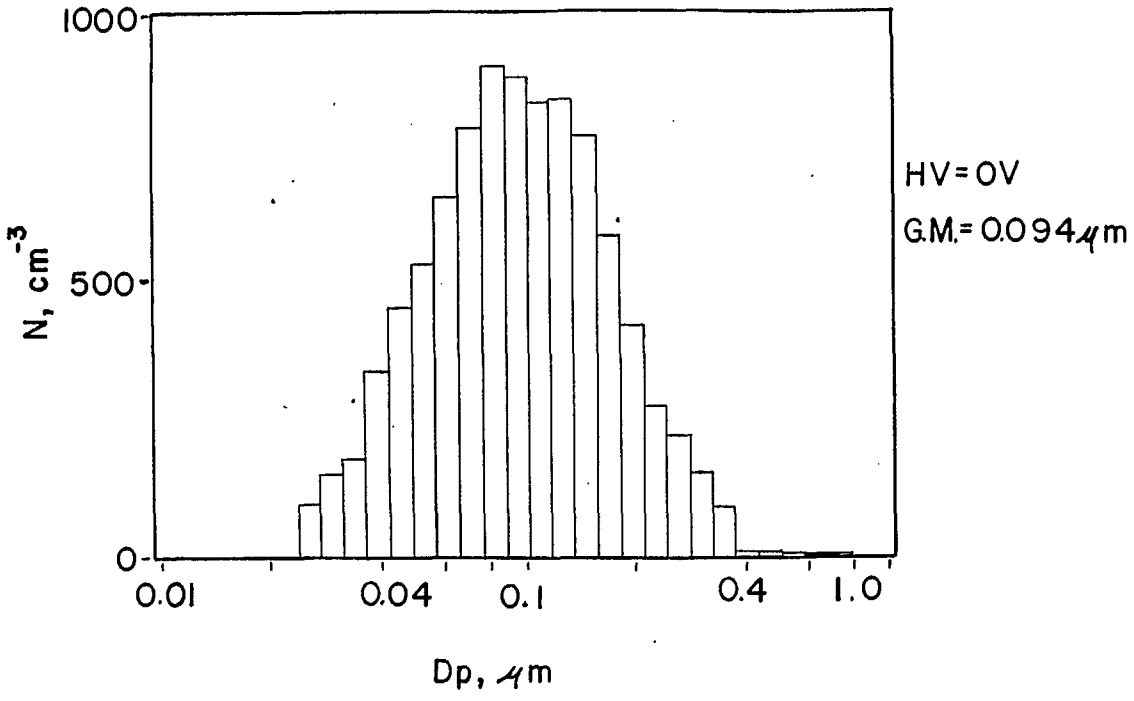
1000
500
0
N, cm-3
0.01
0.04
0.1
0.4
1.0
Dp, μm
HV=0V
G.M.=0.094μm

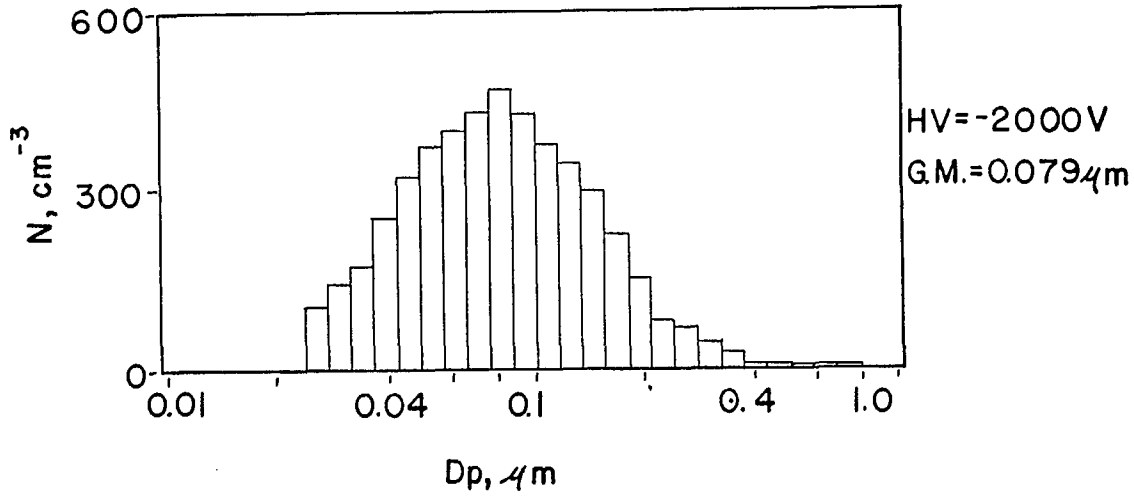
600
300
0
N, cm-3
0.01
0.04
0.1
0.4
1.0
Dp, μm
HV=-2000V
G.M.=0.079μm

Figure 4.

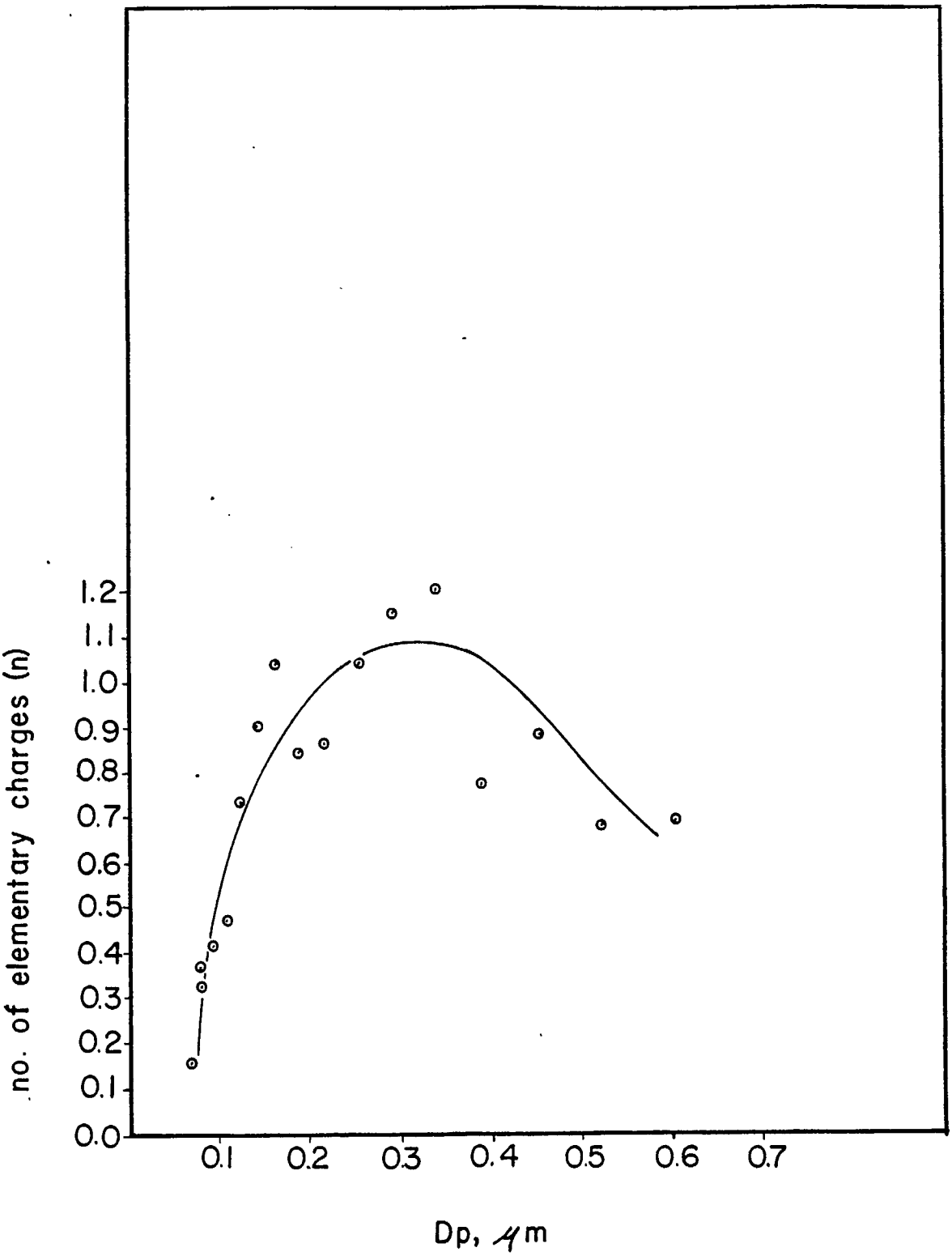
no. of elementary charges (n)
1.2
1.1
1.0
0.9
0.8
0.7
0.6
0.5
0.4
0.3
0.2
0.1
0.0
0.1
0.2
0.3
0.4
0.5
0.6
0.7
Dp, μm

Figure 5.

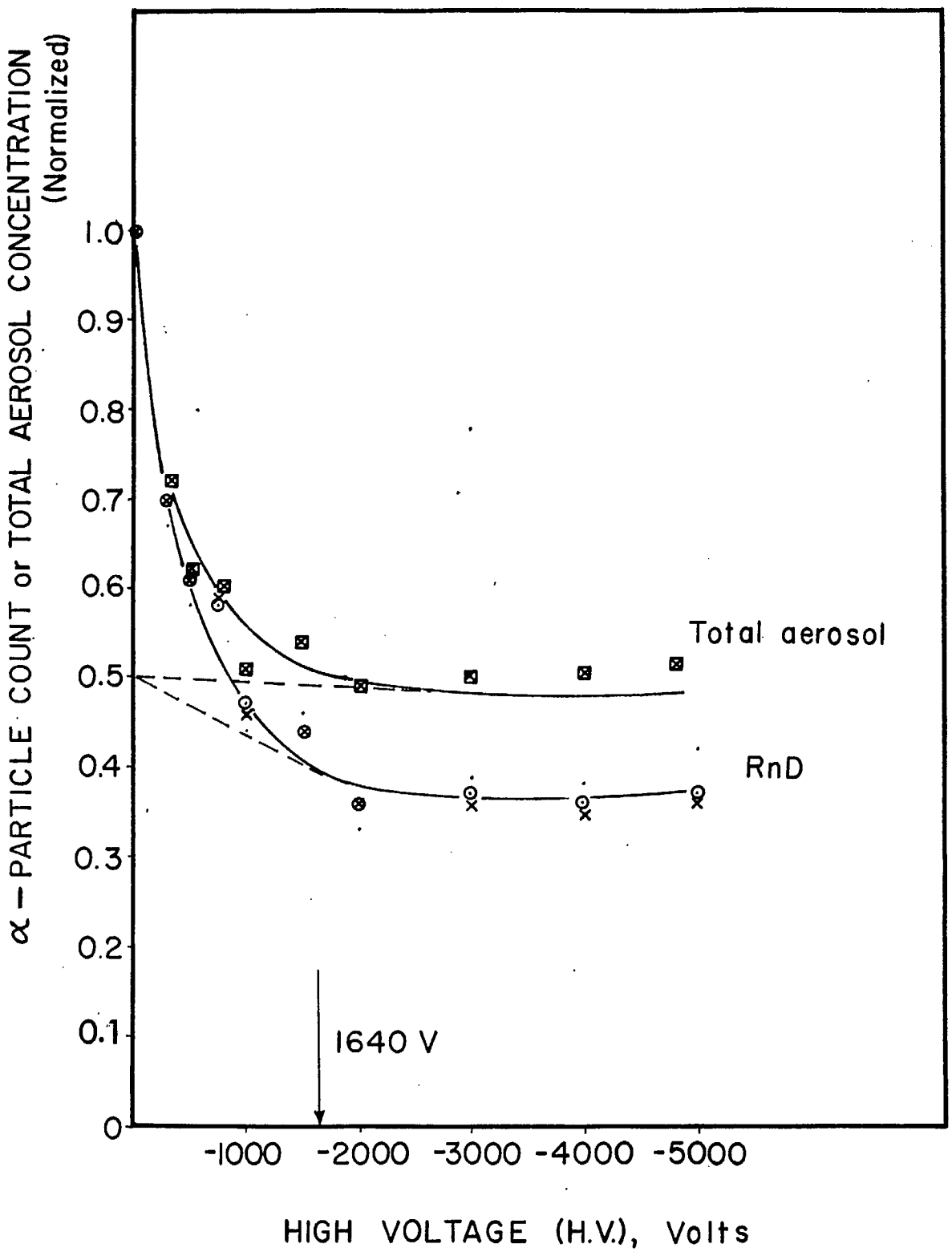
α – PARTICLE COUNT or TOTAL AEROSOL CONCENTRATION (Normalized)
1.0
0.9
0.8
0.7
0.6
0.5
0.4
0.3
0.2
0.1
0
Total aerosol
RnD
1640 V
-1000
-2000
-3000
-4000
-5000
HIGH VOLTAGE (H.V.), Volts

Figure 6.

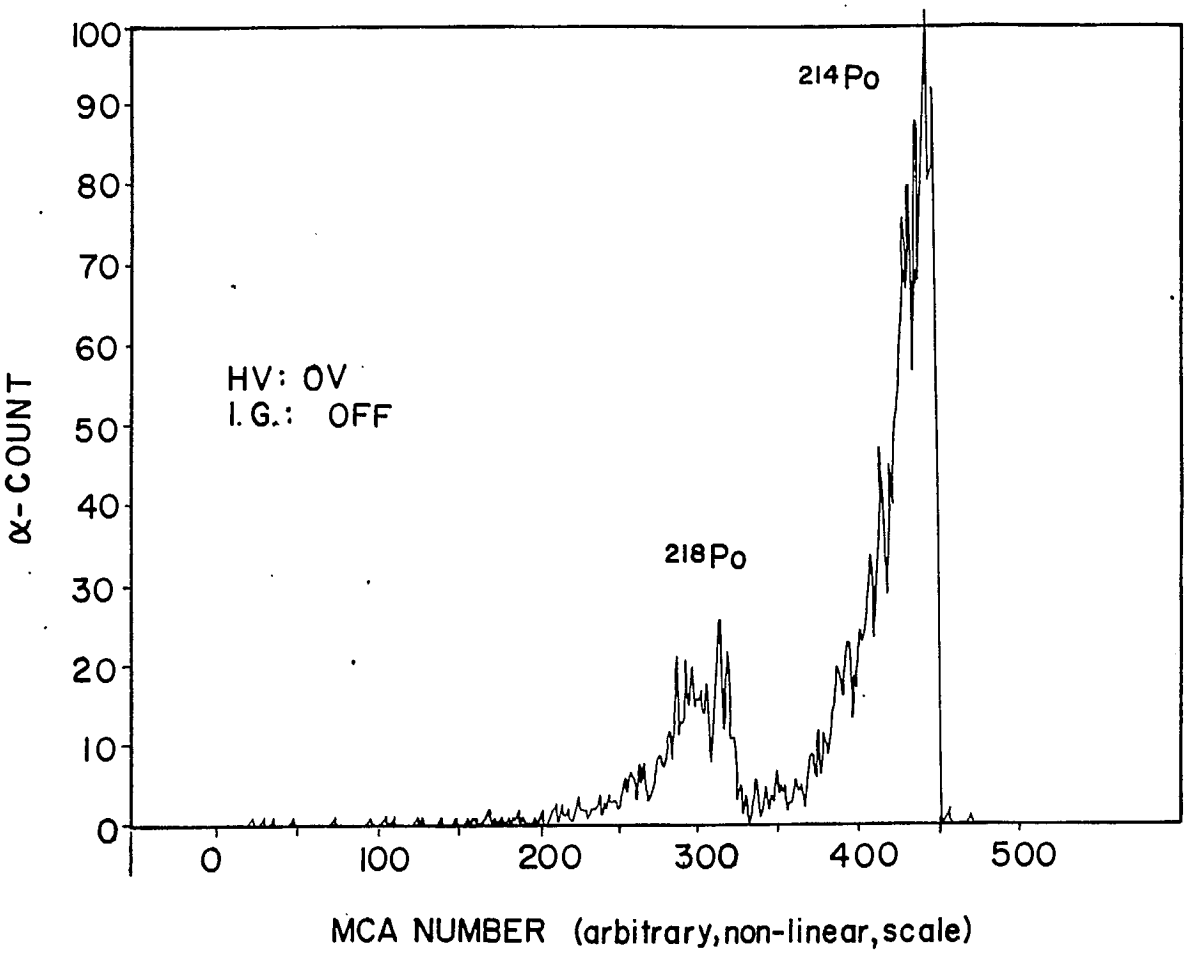
100
90
80
70
60
50
40
30
20
10
0
α-COUNT
HV: 0V
I.G.: OFF
214Po
218Po
0
100
200
300
400
500
MCA NUMBER (arbitrary, non-linear, scale)

Fig. 7 a.

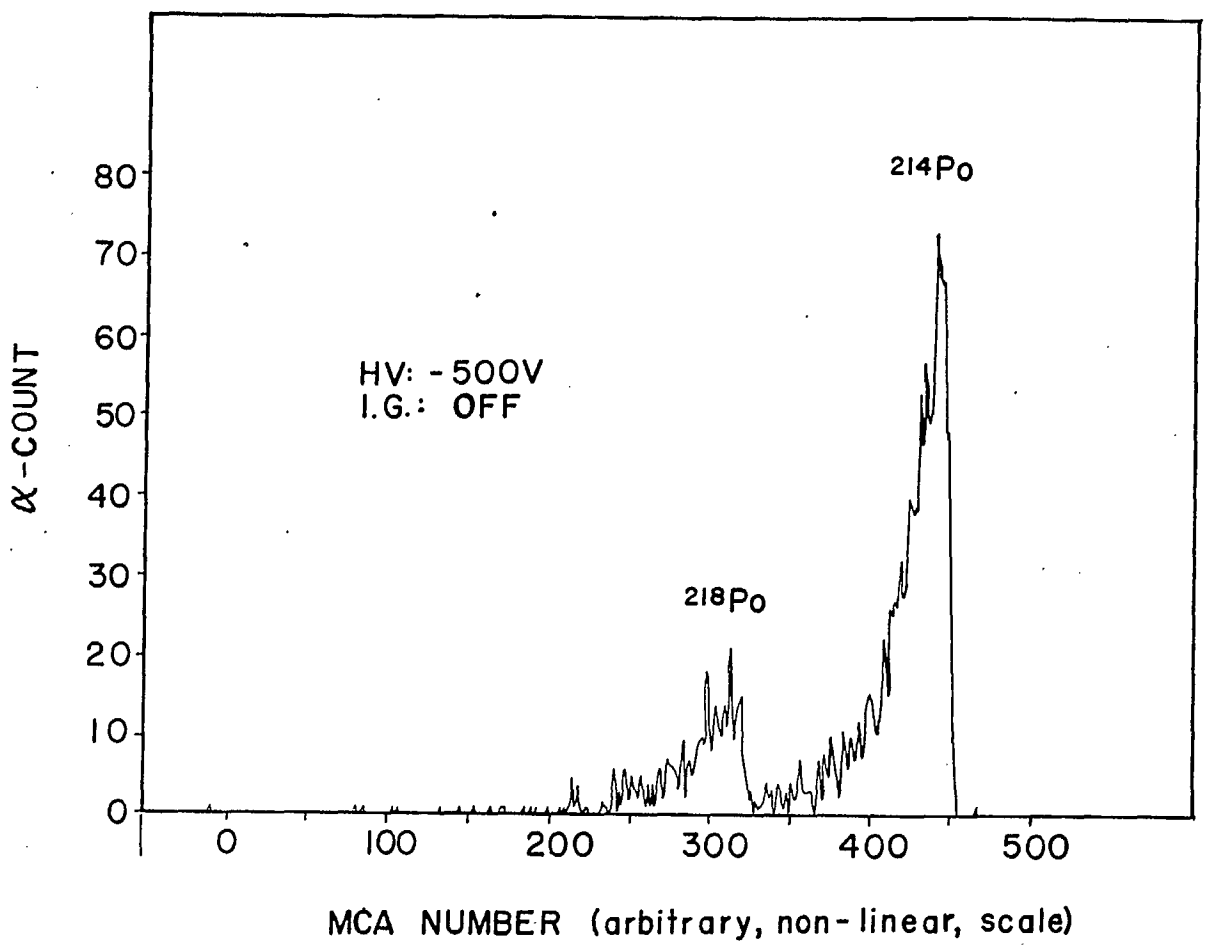
α-COUNT
80
70
60
50
40
30
20
10
0
HV: -500V
I.G.: OFF
214Po
218Po
0
100
200
300
400
500
MCA NUMBER (arbitrary, non-linear, scale)

Fig. 7 b.

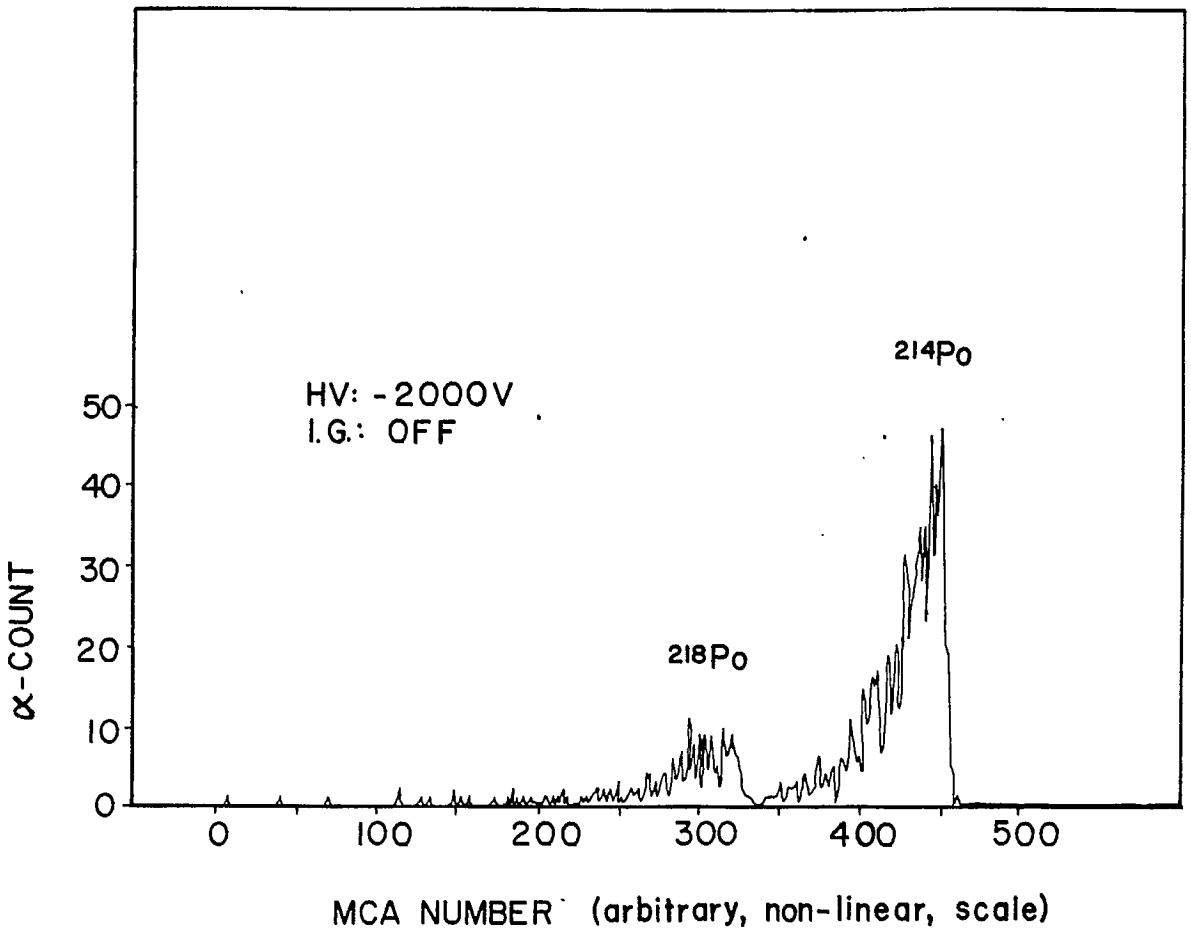
HV: -2000V
I.G.: OFF
214Po
218Po
α-COUNT
0
10
20
30
40
50
0
100
200
300
400
500
MCA NUMBER (arbitrary, non-linear, scale)

Fig. 7 c.

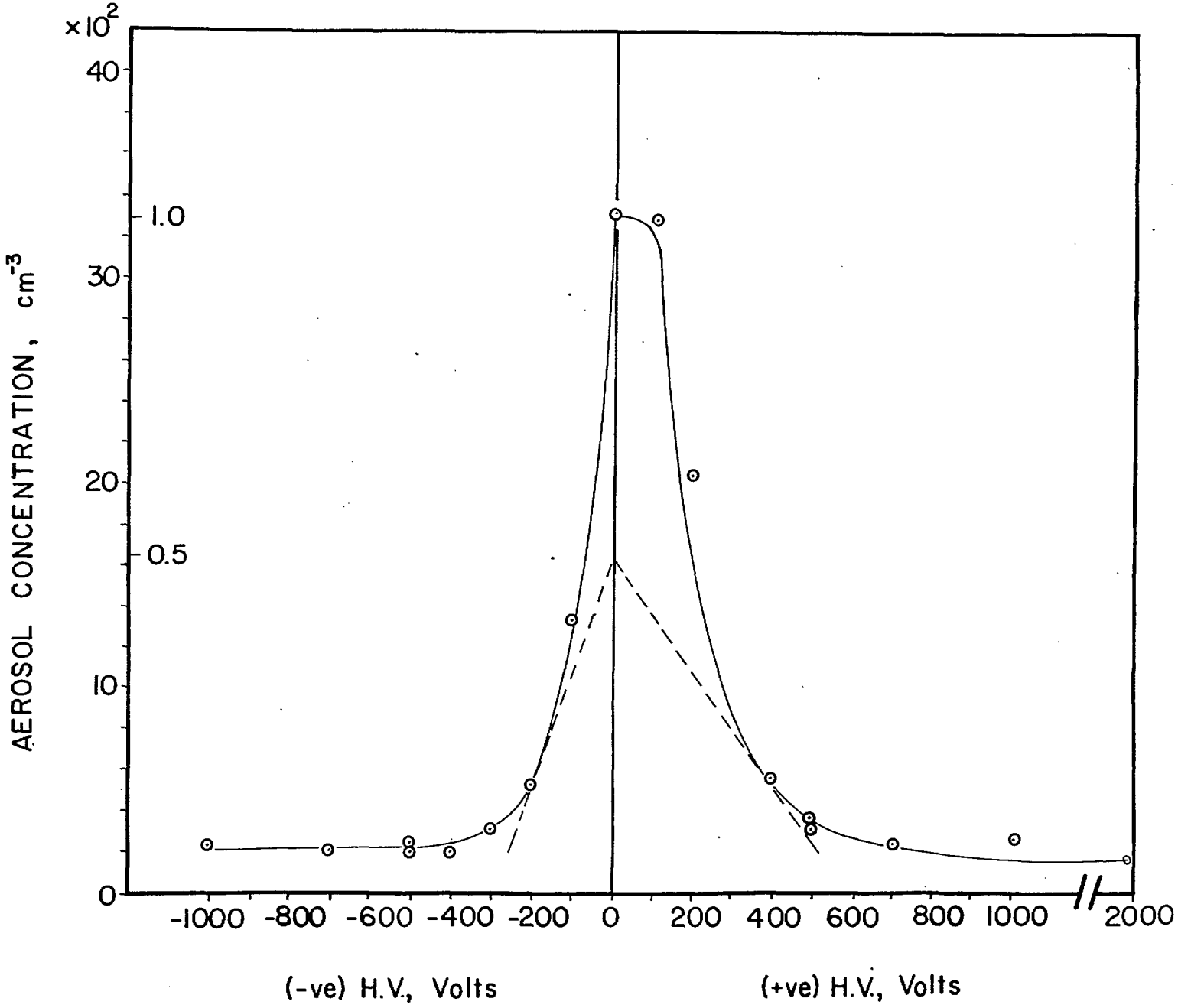
x10²
40
30
20
10
0
1.0
0.5
AEROSOL CONCENTRATION, cm⁻³
-1000 -800 -600 -400 -200 0 200 400 600 800 1000 2000
(-ve) H.V., Volts
(+ve) H.V., Volts

Figure 8.

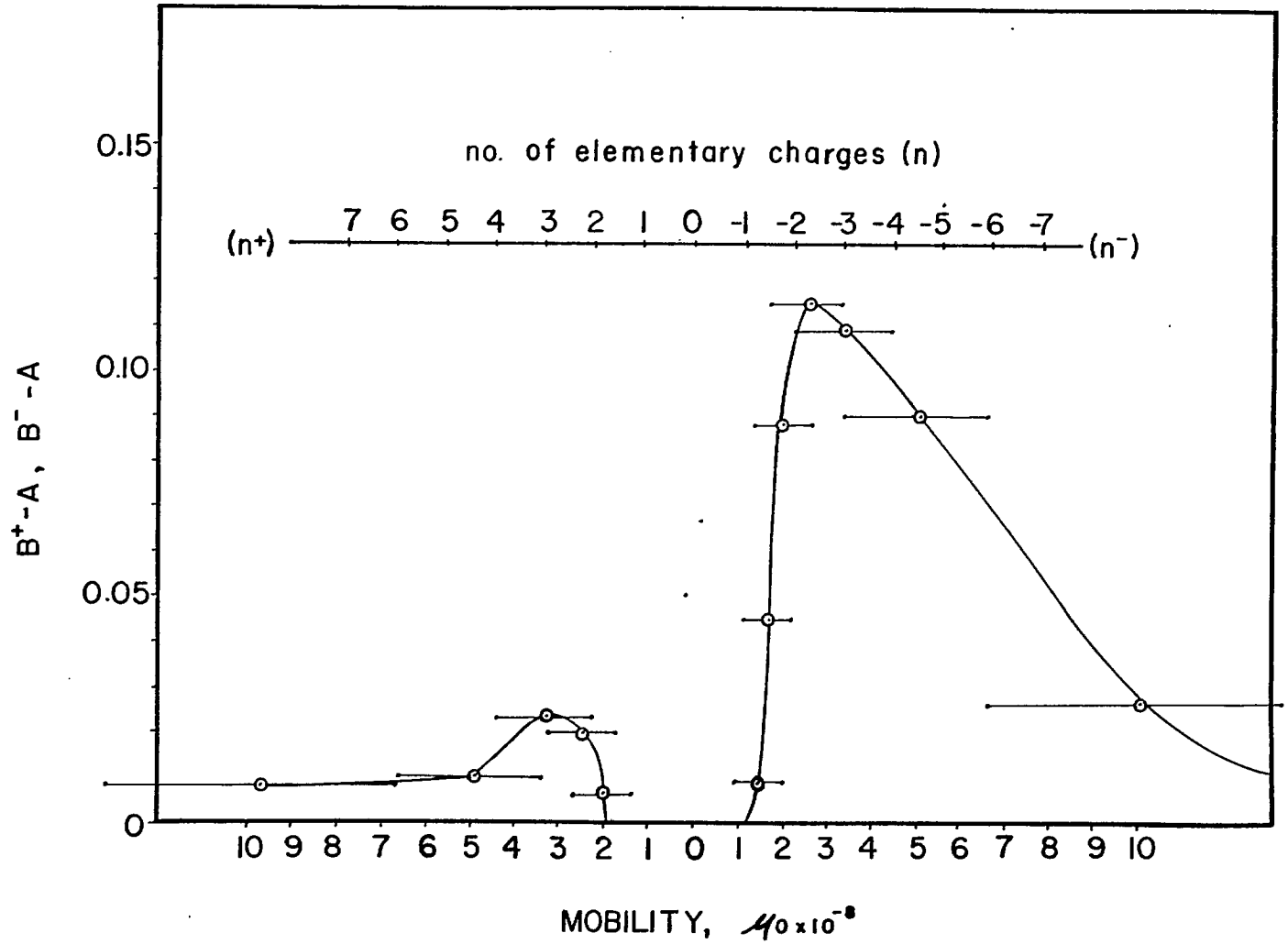
no. of elementary charges (n)
(n+)
7 6 5 4 3 2 1 0 -1 -2 -3 -4 -5 -6 -7
(n⁻)
0.15
0.10
0.05
0
B⁺-A, B⁻-A
10 9 8 7 6 5 4 3 2 1 0 1 2 3 4 5 6 7 8 9 10
MOBILITY, μ₀ x 10⁻⁸

Figure 9.

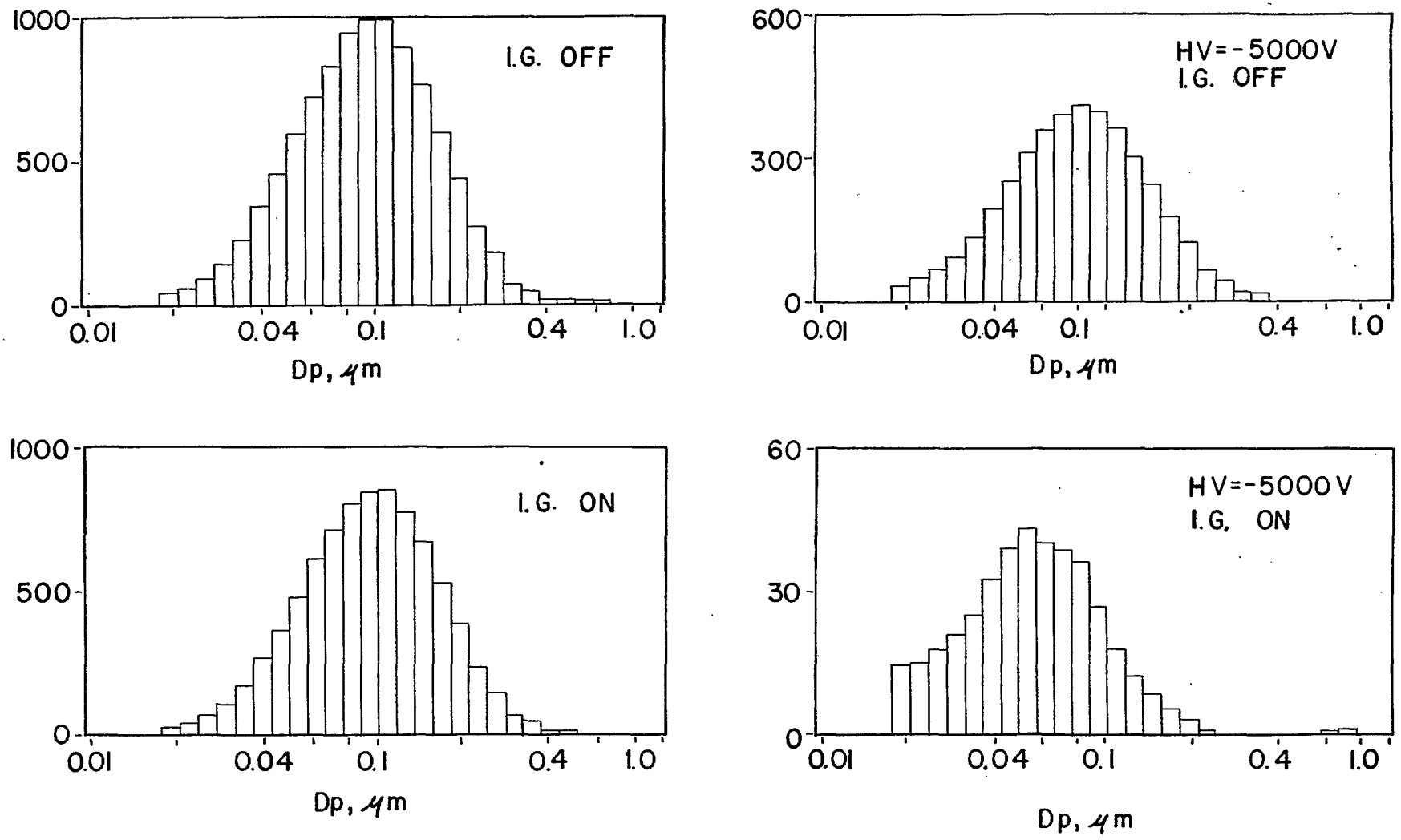
1000
500
0
I.G. OFF
0.01
0.04
0.1
0.4
1.0
Dp, μm
600
300
0
HV=-5000V
I.G. OFF
0.01
0.04
0.1
0.4
1.0
Dp, μm
1000
500
0
I.G. ON
0.01
0.04
0.1
0.4
1.0
Dp, μm
60
30
0
HV=-5000V
I.G. ON
0.01
0.04
0.1
0.4
1.0
Dp, μm

Figure 10.

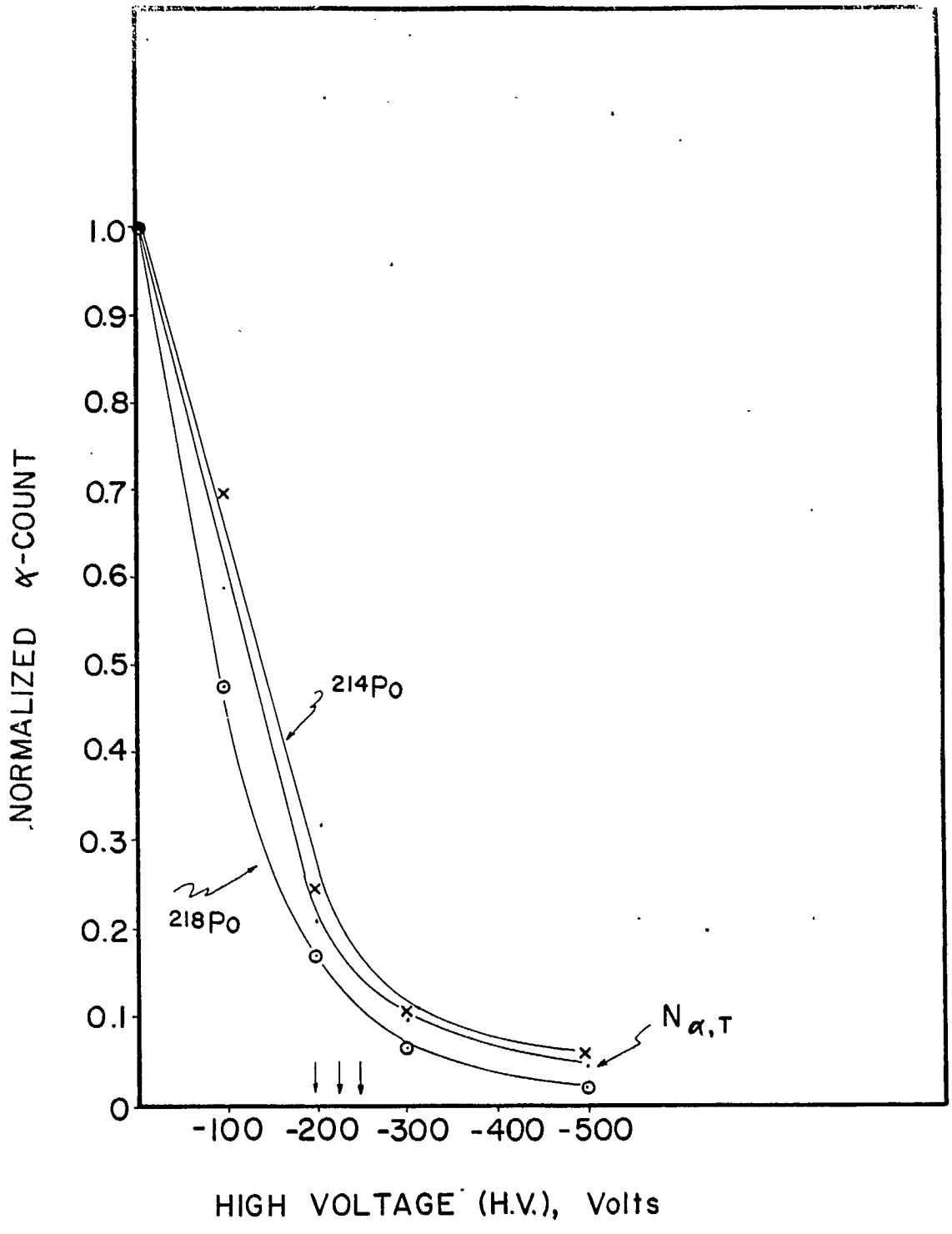
NORMALIZED α-COUNT
1.0
0.9
0.8
0.7
0.6
0.5
0.4
0.3
0.2
0.1
0
214Po
218Po
Nα,T
-100 -200 -300 -400 -500
HIGH VOLTAGE (H.V.), Volts

Figure 11.

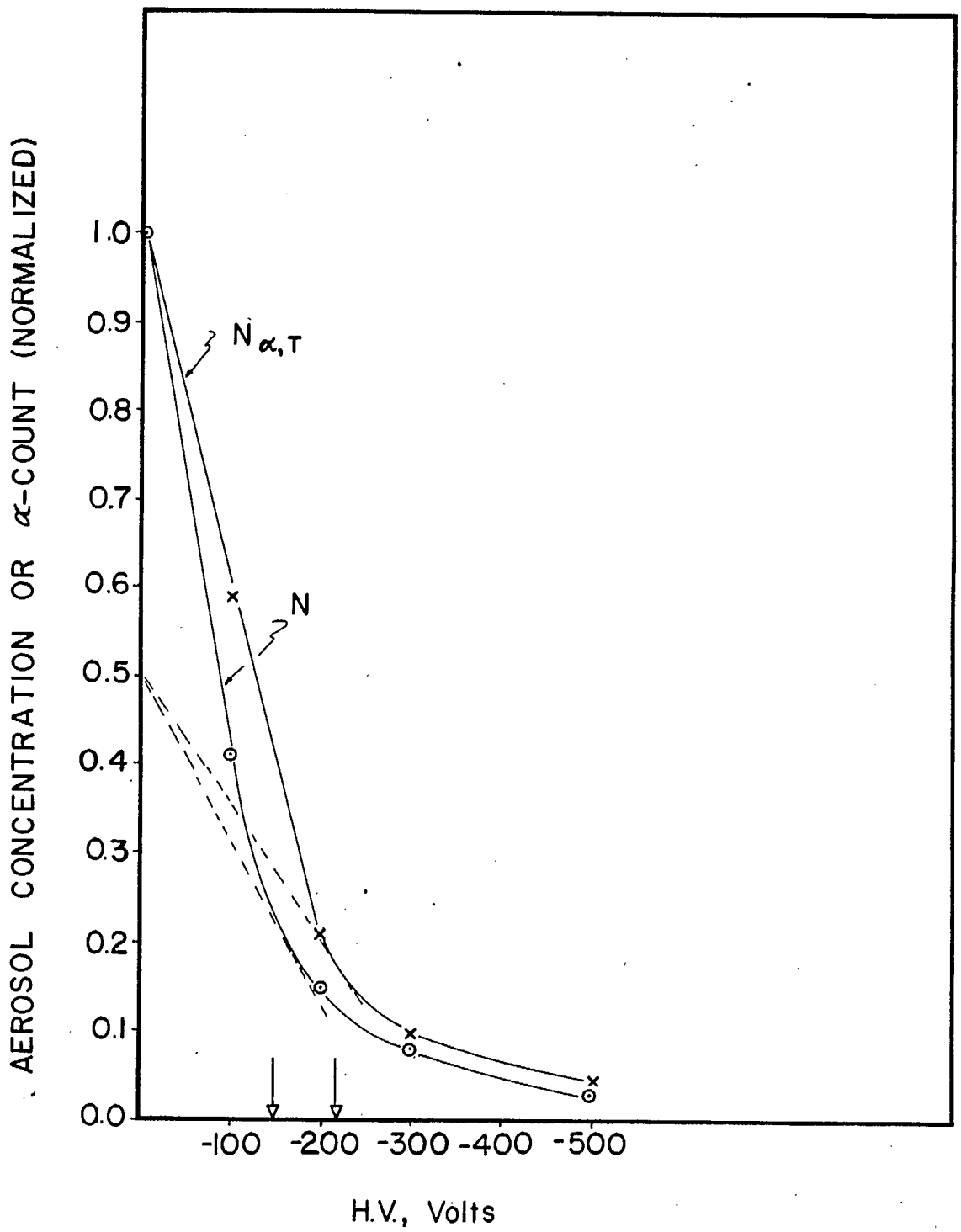
AEROSOL CONCENTRATION OR α-COUNT (NORMALIZED)
1.0
0.9
0.8
0.7
0.6
0.5
0.4
0.3
0.2
0.1
0.0
N α,T
N
-100
-200
-300
-400
-500
H.V., Volts

Figure 12.

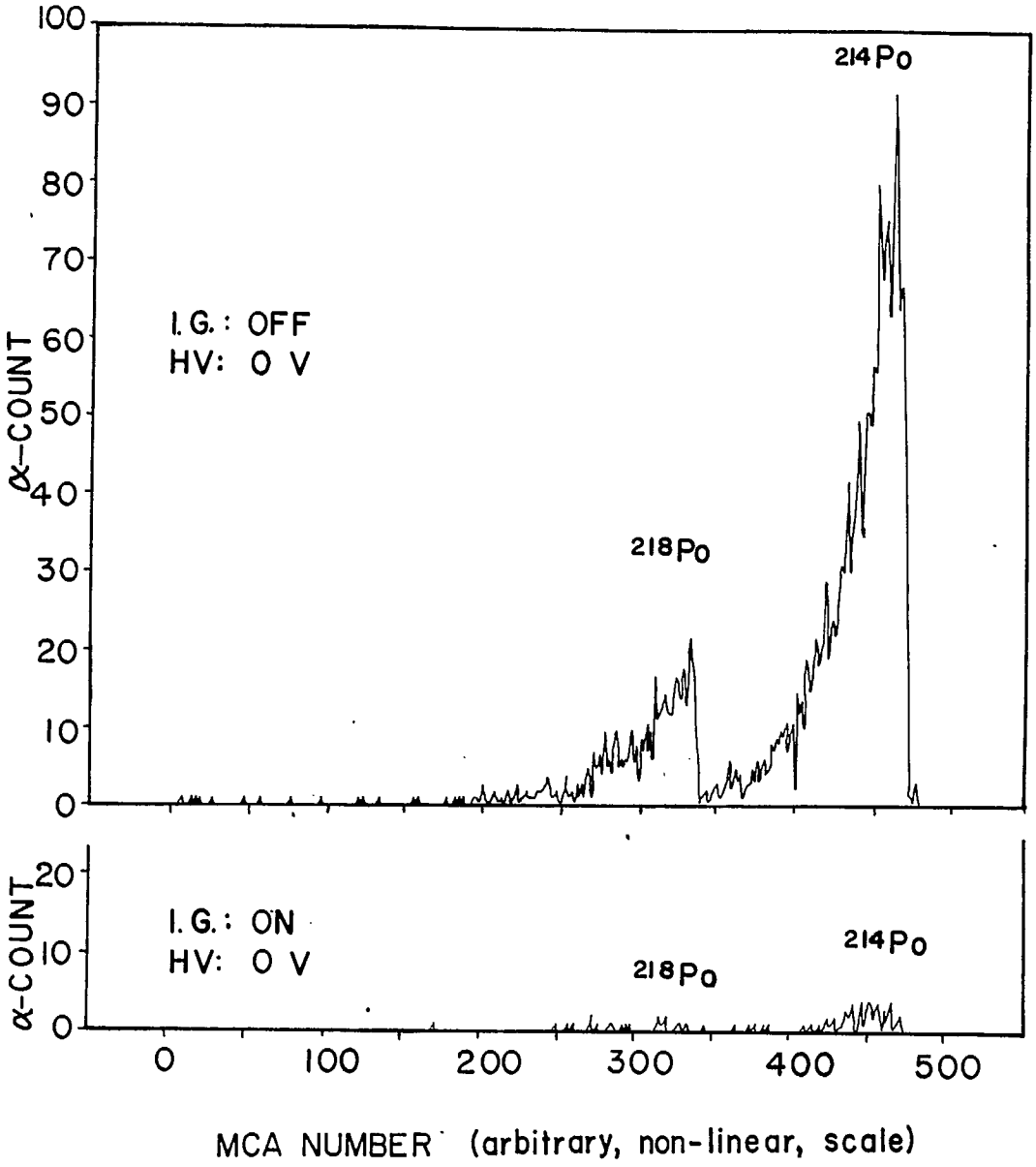
100
90
80
70
60
50
40
30
20
10
0
α-COUNT
I. G. : OFF
HV: 0 V
214Po
218Po
20
10
0
α-COUNT
I. G. : ON
HV: 0 V
218Po
214Po
0
100
200
300
400
500
MCA NUMBER (arbitrary, non-linear, scale)

Figure 13.

## APPENDIX

The detailed analytical and graphical procedure used to deal with asymmetric aerosol charge distributions has been published elsewhere (Johnston 1983). The following are some definitions to clarify the meaning of Figure 9, derived from Figure 8, using Johnston's procedure. For further information the reader is urged to refer to the original publication.

The symbol A stands for A-type experimental 'run', and indicates data obtained when both channels of the split-flow elutriator (SFE) are directed to the aerosol counter, e.g., CNC (see configuration X of Figure 2). Data tabulated under A represent values of the tangent intercept points from the type A curve.

The symbols $B^+$ and $B^-$ refer to data obtained when the aerosol counter samples from the exit channel on the side of the positive and negative electrode of the SFE, respectively (see configuration Y of Figure 2). Data tabulated under $B^+$ and $B^-$ curves represent values of the tangent intercept points on the type $B^+$ and $B^-$ curves, respectively (see Figure 9). (Note: Because of space limitations and simplicity, Tables for A, $B^+$ and $B^-$ are not included in this paper.)